

See discussions, stats, and author profiles for this publication at: <https://www.researchgate.net/publication/44591899>

Grafting of Lanthanide Complexes on Silica Surfaces: A Theoretical Investigation

ARTICLE *in* THE JOURNAL OF PHYSICAL CHEMISTRY A · JUNE 2010

Impact Factor: 2.69 · DOI: 10.1021/jp101495n · Source: PubMed

CITATIONS

10

READS

12

4 AUTHORS:



Iker Del Rosal

Paul Sabatier University - Toulouse III

42 PUBLICATIONS 297 CITATIONS

[SEE PROFILE](#)



Iann C. Gerber

INSA

45 PUBLICATIONS 1,612 CITATIONS

[SEE PROFILE](#)



Romuald Poteau

Paul Sabatier University - Toulouse III

87 PUBLICATIONS 1,145 CITATIONS

[SEE PROFILE](#)



Laurent Maron

Paul Sabatier University - Toulouse III

334 PUBLICATIONS 5,485 CITATIONS

[SEE PROFILE](#)

Grafting of Lanthanide Complexes on Silica Surfaces: A Theoretical Investigation

Del Rosal Iker,[†] Gerber Iann C.,[†] Poteau Romuald,[†] and Maron Laurent^{*‡}

Université de Toulouse, INSA, UPS, LPCNO (IRSAMC), 135 avenue de Rangueil, F-31077 Toulouse, France
and CNRS, UMR 5215 (IRSAMC), F-31077 Toulouse, France

Received: February 18, 2010; Revised Manuscript Received: April 2, 2010

Grafting catalysts on a surface leads to heterogeneous catalysts with well-defined active sites. However, the grafting mode of a lanthanum complex onto silica remains unknown. To shed light on this grafting reaction, different studies have been achieved in the framework of density functional theory. The silica substrate hydroxylated at 700 °C has been simulated both by molecular and periodic models. The created molecular models are in agreement with the rigidity of the ligand, the surface density of silanol groups, and the different spectroscopic data of a silica surface partially dehydroxylated at 700 °C. Two possible models of surface have henceforth been considered: the first one with one isolated silanol and the second one with two vicinal silanols linked by a siloxane bridge. The thermodynamics of a grafting reaction of lanthanum catalysts on these models has also been investigated. This reaction leads to thermodynamically stable structures that reveal different types of grafting: monografted, bigrafted, or bigrafted after breaking of a Si—O—Si bridge. Similarly to experimental approaches, coordination of triphenylphosphine oxide ($O=PPh_3$) has also been considered as a probe of the grafting mode. A good agreement between the theoretical and the experimental spectroscopic values has systematically been found, but none of the grafting modes seem to be more relevant. Accordingly, it is necessary to consider in subsequent studies that all grafting modes coexist, increasing the difficulty to theoretically investigate multistep reactions.

1. Introduction

The surface organometallic chemistry combines the advantages of homogeneous and heterogeneous catalysis. Grafting catalysts on a surface leads to heterogeneous catalysts with well-defined active sites. To achieve this type of catalysis, it is necessary to proceed in different steps. The first step is to analyze the desired chemical transformation and choose the most relevant catalyst to perform the desired reaction. The second step consists in constructing the active sites through a careful understanding of the interaction of molecular complexes with a surface. Finally, the third step entails the testing of these catalysts in order to gather data on their activities, selectivities, and lifetimes, which will be used to decide upon a strategy to improve the catalytic system. To have a better understanding of the system, the choice of the support plays an important role. One of the most used support is silica. It is a good candidate because it respects the most important criteria of the surface organometallic chemistry: the support does not generate parallel reactions and there is a reasonable knowledge of its surface structure in order to understand its reactivity with an organometallic complex. More recently, quantum chemistry studies have helped to advance significantly the understanding of properties of silica. Two strategies have been adopted to compute the electronic structure of silica and its defects: cluster models^{1–6} and periodic supercell models.^{7–10} In all these studies, the surface is considered as a large siloxy ligand and the grafting mode is not studied. The catalyst is simply grafted in a terminal position, prior to reactivity studies. It should be noticed that experimental data do not give enough information to determine

the grafting mode. For instance, the dehydroxylation temperature allows for the control of the surface density of the hydroxyl groups before the grafting reaction. This reaction can be followed by infrared spectra by monitoring the disappearance of the ν_{OH} signal corresponding to the surface silanols consumed. In a second time by the combination of infrared, ²⁹Si MAS NMR spectroscopy as well as ¹H NMR spectroscopy data in the case of paramagnetic materials, it is possible to estimate¹¹ the grafted catalyst density by nm². However, although the grafting mode remains unknown, it is often supposed that the catalyst is monoanchored.^{12,13} In this work, we will show that several grafting modes can exist and that all these modes agree with the experimental data. This study will be divided into two parts.

The first part is devoted to creating a cluster model of a silica surface partially dehydroxylated at 700 °C, compatible with different structural and spectroscopic experimental data. The modeling of amorphous supports is still a challenge for computational chemists, because of the complexity of amorphous systems that would require expensive calculations. In general, the computational modeling of amorphous solids using periodic boundary conditions is usually considered as the most relevant approach. Nevertheless, a study carried out by Solans-Monfort et al.¹⁴ has shown that the experimental characteristic data are well reproduced and nearly identical for cluster models and periodic systems. In this study, we have chosen the molecular approach to model the silicate surface, which allows easier investigations of multistep reactions mechanisms.

The second part of our study involves another important step of the surface organometallic chemistry, which is the interaction between the catalyst and the support. The silica-supported catalyst is prepared by reaction of $La(N(SiMe_3)_2)_3$ ¹⁵ with a silica partially dehydroxylated at 700 °C. Lanthanum catalysts are usually used in different reactions such as the monoaddition of terminal alkynes or nitriles¹⁶ as well as the hydridosilylation of

* To whom correspondence should be addressed. E-mail: laurent.maron@irsamc.ups-tlse.fr.

[†] LPCNO (IRSAMC).

[‡] INSA.

alkene or the dimerization of alkynes.¹¹ Experimental work, involving IR and NMR spectroscopy, was carried out to determine the nature of the grafting mode on the surface. In particular, coordination of triphenylphosphine oxide ($O=PPh_3$) was carried out by Gauvin et al.,¹¹ and different IR and NMR spectra have been determined. The different optimized structures will be compared on the basis of these chemical shift values and vibrational frequencies. The knowledge of the catalyst grafting mode is crucial because it conditions all the parameters of reaction pathways: kinetic and thermodynamic data, regioselectivity, and stereoselectivity.

2. Methodological Details

All DFT calculations were performed with Gaussian 03.¹⁷ Calculations were carried out at the DFT level of theory using the hybrid functional B3PW91.^{18–23} Geometry optimizations were achieved without any symmetry restriction. Calculations of vibrational frequencies were systematically done in order to characterize the nature of stationary points. Stuttgart effective core potentials²⁴ and their associated basis set were used for silicon and lanthanum. The basis sets were augmented by a set of polarization functions ($\zeta_d = 0.284$ for Si and $\zeta_f = 1.000$ for La). Hydrogen and oxygen atoms were treated with 6-31G(d,p) double- ζ basis sets.^{25,26} Among the various theories available to compute chemical shielding tensors, the gauge including atomic orbital (GIAO) method has been adopted for the numerous advantages it presents.^{27–31} The electron density and partial charge distribution were examined in terms of localized electron-pair bonding units by using the NBO program.^{32,33} Through this method, the input atomic orbital basis set is transformed via natural atomic orbitals (NAOs) and natural hybrid orbitals (NHOs) into natural bond orbitals (NBOs), which correspond to the localized one center (“lone pair”) and two-center (“bond”) elements of the Lewis structure. All possible interactions between “filled” (donor) Lewis-type NBOs and “empty” (acceptor) non-Lewis NBOs orbitals, together with their energetic quantification (stabilization energy), have been obtained by a second-order perturbation theory analysis of the Fock matrix. Only stabilization energy higher than 10 kcal. mol⁻¹ has been considered.

The periodic DFT geometry optimizations and energetic calculations were carried out using the Vienna ab initio simulation package.^{34,35} The code uses the full-potential projector augmented waves (PAW) framework.^{36,37} Exchange-correlation effects have been approximated using the PBE³⁸ functional and applied in spin-polarized calculations. Considering PAW calculations, a kinetic energy cutoff of 400 eV was found to be sufficient to achieve a total energy convergence within several meV, after careful analysis of the k -points sampling issue. A Γ -centered ($4 \times 4 \times 1$) grid of k -points³⁹ was used to sample the reciprocal space combined with a Gaussian smearing of 0.2 eV width for partial occupancies in geometry optimizations, and a ($7 \times 7 \times 1$) k -points grid and the tetrahedron method of Blöchl⁴⁰ for the determination of partial occupancies were used to yield accurate energy differences. All relaxed atoms were free to move until forces on any direction were less than 0.03 eV/Å. The repeated images are separated in the z direction by a vacuum of 16.4 Å for a total height cell of 24.5 Å.

3. Creation of the Surface Model

3.1. Experimental Data. Silica surfaces can be natural or synthetic but also crystalline (quartz, cristobalite, edingtonite, etc.) or amorphous. They can have different structures depending on the temperature and the pressure.^{41,42} Nevertheless, all

crystalline forms involve tetrahedral SiO_4 units linked together by shared vertices, in different arrangements. Silicon atoms are connected by an oxygen bridge, named siloxane bridge. These bridges are not reactive, so it is necessary beforehand to treat the surface with water in order to break these bonds and to create reactive functional groups that will anchor the catalysts.

A detailed review of the interactions between water and solid surfaces is given in refs 43 and 44. All theoretical studies of the hydroxylation process of silica surfaces^{7,45–47} agree to state that the attack of a water molecule on a Si—O—Si linkage leads to the formation of two silanol groups. Depending on the distance between the hydroxyl groups, three different repartition of silanol groups can be obtained: isolated, geminal with two hydroxyl groups on the same silicon, or vicinal with two hydroxyl groups in two neighbor silicones. IR spectroscopy studies^{48–50} show that the vibrational frequencies associated with the hydroxyl group lie between 3500 and 3750 cm⁻¹, the lowest values corresponding to silanols involved in hydrogen bonds. However, after treating the silicate surface at 700 °C, only one sharp symmetrical band remains at 3747 cm⁻¹. This shows that for a SiO_2 –700 surface, the silanol groups are sufficiently far from each other so that they can be considered as isolated.

The silanol groups are very reactive and will be involved in interactions and chemical reactions at the silica surface. For this reason, it is necessary to determine the number of silanol groups on the silicate surface. Several experimental studies were carried out for that purpose: Raman spectroscopy,^{51–53} thermogravimetric analysis,^{54,55} and Karl Fischer titration^{56–58} or other chemical methods.^{55,59,60} Moreover, one of the most relevant study to quantify the number of silanol groups was carried out by Zhuravlev.⁶¹ This study is based on an exchange reaction between hydrogen and deuterium atoms and mass spectroscopy measurements. This method has the advantage that only the surface silanols are taken into account, and not the subsurfacic silanols or adsorbed water. This study was realized on more than 100 samples, with silicas of different nature and characteristics.^{50,59,62–65} The conclusion of this study is that the concentration of surface silanols can be considered as a constant equal to $4.6 \pm 0.5 \text{ OH} \cdot \text{nm}^{-2}$ at 200 °C. Moreover, by the combination of the Zhuravlev model with IRTF integration, based on the integration of the surface of each vibration band corresponding to the silanol groups, and MAS ²⁹Si NMR data, it is possible to obtain the proportion of each type of silanol group, that is, isolated, geminal or vicinal, as a function of the temperature.⁶⁶ As expected, the silanol density decreases as a function of temperature. In addition, no vicinal silanol groups are expected to be present on the surface, whereas isolated silanol groups are observed in higher yield than geminal groups.

In our study we will consider silica treated at 700 °C, which, according to the work of Vansant et al.,⁶⁶ yields to a silanol surface density close to $1.15 \text{ OH} \cdot \text{nm}^{-2}$, with a 0.90/0.25 isolated/geminal ratio. In other words, this density corresponds to silanol groups separated by an average distance of 5–6 Å, and it ensures homogeneous active sites.

3.2. Preliminary Surface Models. We shall now present two models for silica surface that were first investigated. Although they will not be considered in the next sections, their intrinsic limitations are instructive. For the first model, (Figure 1a) the four silicon atoms are linked by siloxane bridges. The four hydroxyl groups of the top represent the silanol groups resulting from the treatment by water, and the four bottom hydroxyl groups are used to avoid dangling bonds. The important asset of this model is the small number of atoms and thus the reduced computation time. However, the lack of a second silica layer

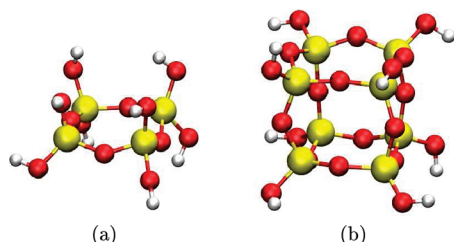


Figure 1. First surface silicate models made up of four (a) and eight (b) silicon atoms.

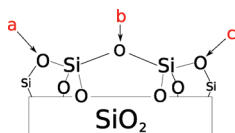


Figure 2. Neighboring siloxane bonds (named **a**, **b**, and **c**) possibly attacked by water.

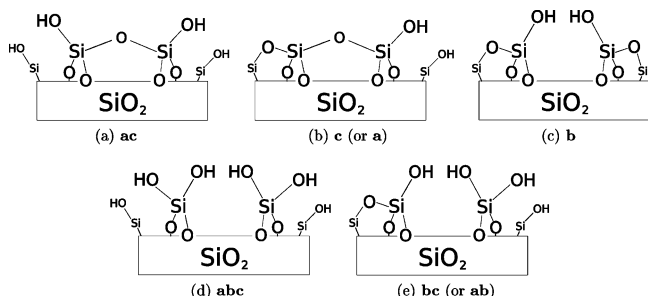


Figure 3. Various forms obtained after breaking of one or more siloxane linkages. The labels **a**, **b**, and **c** refer to the attack pathways shown in Figure 2.

makes this model too flexible, thus leading to spurious interactions, in particular with the hydroxyl groups used to saturate the cluster.

The second cluster (Figure 1b) is a larger model with eight silicon atoms, forming a cage in order to improve the rigidity of the cluster. As for the first model, four hydroxyl groups are used to saturate the model (bottom), and the other hydroxyl groups are the result of the treatment by water. This model is similar to the silsesquioxanes compounds^{67–70} often experimentally considered as models for silica surfaces. These compounds were synthesized and have a close geometric similarity to the structure of idealized trisilanol sites available on cristobalite (111) and tridymite (0001). Nevertheless, there still remains a problem that is the density of silanol groups. For both models, the distance between two silanol groups is 3 Å, which is less than with the experimental values.

3.3. Adopted Silica Surface Model. Another possibility is to create a model inspired by the studies of Mortreux and Gauvin.^{11–13} They showed that, at 700 °C, water molecules attack on small isolated silica islands on the surface, containing one or two silanol sites. In this case water can attack on three neighboring O–Si–O bridges (Figure 2) leading to five possible structures according to the number and position of bridges actually broken by the hydroxylation process (Figure 3). However, since according to surface density data the silanol groups are expected to be rather far away from each other on a SiO₂–700 surface, models **abc** and **bc** can be considered as less relevant than the three other ones. However, they should be more appropriate as silica surface models treated at lower temperatures.

Figure 4 presents the optimized geometry of the three remaining models, namely, **ac**, **c**, and **b**. The two upper silicon

atoms, connected by a siloxane bridge, roughly represent the emerged part of the silica surface, surrounded by a layer built around four silicon atoms, themselves connected to O–SiH₃ groups, which represent the continuity of the surface. The presence of terminal silyl groups avoids spurious coordinations observed with the simple surface models (Figure 1). Finally, a second layer formed by two silicons is added to increase the rigidity of the model. Both silicons are connected to hydroxyl groups to saturate the model. The rigidity of the cluster and the large distance between the silanol groups and the bonding site ensures that an artifactual coordination of these groups with a grafted complex is avoided. One should pay attention that SiH₃ groups must be added to saturate the lateral siloxane bridges that are not broken by water in **c** and **b** models.

Could these three models be considered as relevant models of surfacic small islands in amorphous silica materials? A partial answer should be given by comparing experimental^{48–50} and calculated vibrational frequencies of the hydroxyl groups present on the defect. As can be seen in Table 1, the experimental value of 3747 cm⁻¹, assigned to isolated silanol groups, compares well with theoretical calculations—3771, 3770, or 3763 cm⁻¹ depending on the model—versus 3747 cm⁻¹. The frequencies calculated for two silanol groups in vicinal position linked by a siloxane bridge (**ac** model) are almost identical to those calculated for an isolated silanol group (**c** model). Model **b** presents one frequency at 3516 cm⁻¹, corresponding to an hydroxyl group involved in an hydrogen bond. Although, the hydroxyl groups are coordinated to the same silicon atoms in **ac** and **b** models, the breaking of the central siloxane bridge in **b** involves the formation of an hydrogen bond between these groups, characterized by an infrared OH fingerprint at 3516 cm⁻¹. Since, it has been recalled in Section 3.1 that SiO₂–700 silicate exhibits only one sharp band at 3747 cm⁻¹, model **b** is incompatible with experimental data and must be excluded from the set of representative hydroxylated silica at 700 °C.

MAS ²⁹Si NMR spectroscopy is another possibility to prove the accuracy of the two models such as a realistic silicate surface models. Indeed, the silicon NMR has become a standard method to structurally characterize the silicate surfaces. Different studies have shown that theoretical values of MAS ²⁹Si NMR are in very good agreement with the experimental value as for the cluster models^{5,6} as for the periodic models.¹⁰ In our case, the two models present different silicon atoms: one isolated silanol (**c** model) and two vicinal silanol (**ac** model). Instead of calculating chemical shifts as $\delta = (\sigma_{\text{ref}} - \sigma)10^6$ ppm, with the reference chemical shielding (σ_{ref}) are the value of the silicon atom in a tetramethylsilane (TMS) molecule. Experimental and calculated MAS ²⁹Si NMR data are summarized in Table 2.⁷¹ NMR spectroscopy does not allow differentiation of silicon atoms involved in isolated silanols or in vicinal silanols, since they similarly resonate, with $\delta = -99$ ppm. Nevertheless, they can be distinguished from silicon atoms involved in siloxane bonds, which are more shielded by 10 ppm ($\delta = -109$ ppm). We shall now recall that an agreement of theoretical chemical shifts with 10–20% deviation from experiment is often considered as good. According to that criterion, NMR calculations performed in the 6-31G** basis set can be considered as weakly accurate, although the relative difference between the different bonding situations is very well reproduced: $\Delta\delta$ is found to be 0 ppm between isolated and vicinal silanol groups, whereas silicon atoms in siloxane are shifted upfield by 8 ppm. NMR data obtained in a larger basis set, namely, cc-pvtz, are in a somewhat better agreement with experiments. Although silicon chemical shieldings vary as a function of the basis set by more

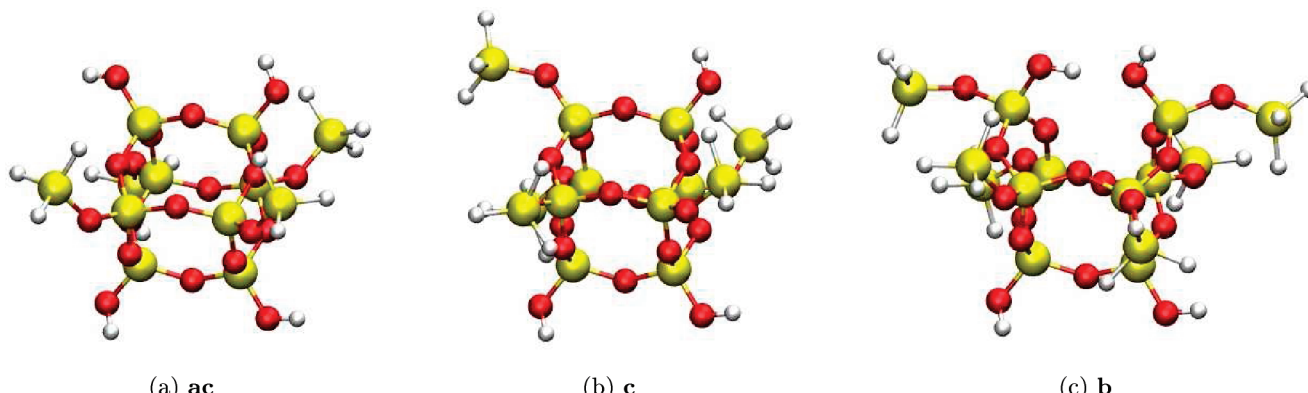


Figure 4. Representation of the three more realistic models of the SiO₂-700 surface. Panels a–c correspond to Figure 3, Panels a–c, respectively. The labels **a**, **b**, and **c** refer to the attack pathways shown in Figure 2.

TABLE 1: Experimental (After Treatment at 700°C) and Calculated Values for the Vibrational Frequencies (in cm^{-1}) of the Surfacic Hydroxyl Groups for the Three Different Surface Models

model	ac	c	b	exp.
$\nu_{\text{O-H}}$	3771/3769	3770	3763/3516	3747

TABLE 2: Comparison between the Theoretical and the Experimental ^{29}Si NMR Chemical Shifts (δ) and Chemical Shieldings (σ , in ppm) for Different Silanol Groups^a

	silanols	isolated	vicinal	siloxane
Exp. ^{29}Si NMR a c	δ	-99	-99	-109
	σ		489.5/436.7	
	δ		-76.2/-83.9	
c	σ	489.4/436.9		496.7/444.7
	δ	-76.2/-84.0		-83.4/-91.9

^a Chemical shifts are given with respect to TMS (theoretical chemical shielding: 413.2 ppm/352.9 ppm according to the basis set). The two theoretical values for each situation correspond to calculations performed with 6-31G** (left) and cc-pvtz (right) basis sets.

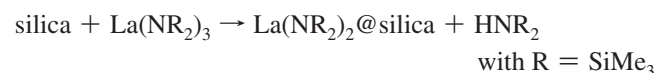
than 50 ppm, calculated chemical shifts are shifted downfield by 10 ppm. Theoretical results are now fairly accurate with respect to experimental values with an error close to 15%. The assignation of the chemical shifts to the different bonding situations is still very accurate, with $\Delta\delta$ 0.1 ppm between isolated and vicinal silanols and $\Delta\delta$ 7.9 ppm between silanols and siloxane. In summary, we obtain the same chemical shieldings for isolated and vicinal silanols, whereas silanol groups and siloxane bridges can be differentiated whatever the basis set is. Similarly to experiments, NMR calculations are a good probe of the local environment of silicon atoms in silica treated surfaces.

3.4. Comparison with Edingtonite (100). Solans-Monfort et al.¹⁴ have shown that geometries and stretching frequencies of silica-grafted Rhenium complexes are nearly identical for cluster models and periodic systems. Although it seems tempting to systematically restrict theoretical studies of grafted complexes to molecular models on the basis of these previous results, one should notice that a single grafting assumption has only been considered. We shall thus carefully achieve comparisons between molecular models and plane-wave periodic calculations in the context of various grafting modes. The first step is to consider hydroxylated silica. The considered periodic system is edingtonite,^{72–74} obtained by cutting the edingtonite bulk parallel to the (100) face. The surface is terminated by hydroxyl groups, and the unit cell includes four edingtonite building blocks of formula $(\text{SiO}_2)_5$ (see Figure 5).

The experimental silica is amorphous, with local crystalline order and a well-characterized density of silanol groups at the surface. The choice for the periodic system, among edingtonite, crystobalite, quartz, etc., should agree with those parameters. Edingtonite has four silanol groups separated from each other by about 6 Å. In this case, the density of silanol groups is similar to that observed experimentally, contrarily to the cristobalite case. In addition, Edingtonite presents isolated silanols so that we can compare it with the **c** model only. The first comparisons we can make between the edingtonite₁₀₀ and the **c** model concerns the local geometry of the isolated silanol. For both systems (Table 3), distances and angles characteristic of silanol groups are similar despite different computational details. In the case of **c** model, the Si_n—O_{2,3,4} distances will be slightly longer by 0.02 Å relatively to edingtonite₁₀₀, whereas the H—O and Si₁—O₁ distances are almost the same. Angles are also very close, with differences below 4°. The value of the vibrational frequency of the hydroxyl group for these two systems is also close: 3695 vs 3770 cm⁻¹, respectively, for edingtonite₁₀₀ and the **c** model. It is slightly functional dependent, with $\nu_{\text{O}-\text{H}} = 3634 \text{ cm}^{-1}$ at the DFT-PBE level of calculation versus 3770 cm⁻¹ at the DFT-B3PW91 level of calculation. Considering that the grafting site is identically described at the two levels of calculation, one can expect similar results in the case of grafted complexes, provided that the molecular model remains relevant.

4. Grafted Lanthanide Complexes

4.1. Grafting Reaction of an Lanthanum Complex onto Cluster Models. To understand the surface chemistry of silica and validate the molecular surface models, we shall first study the grafting of a lanthanide complex onto silica. As demonstrated experimentally by Anwander et al.,^{75,76} lanthanide amides can be grafted onto silica. The grafting occurs through a protonolysis of the Ln-N bond by surface silanols, which generates a covalent $\equiv\text{Si}-\text{O}-\text{Ln}$ bond:



where the lanthanum complex loses one amino group, which combines with an H atom originating from the Si-OH grafting site.

The experimental silyl groups R is modeled by hydrogens. This reaction is studied for the **a**c and **c** models of silica surface.

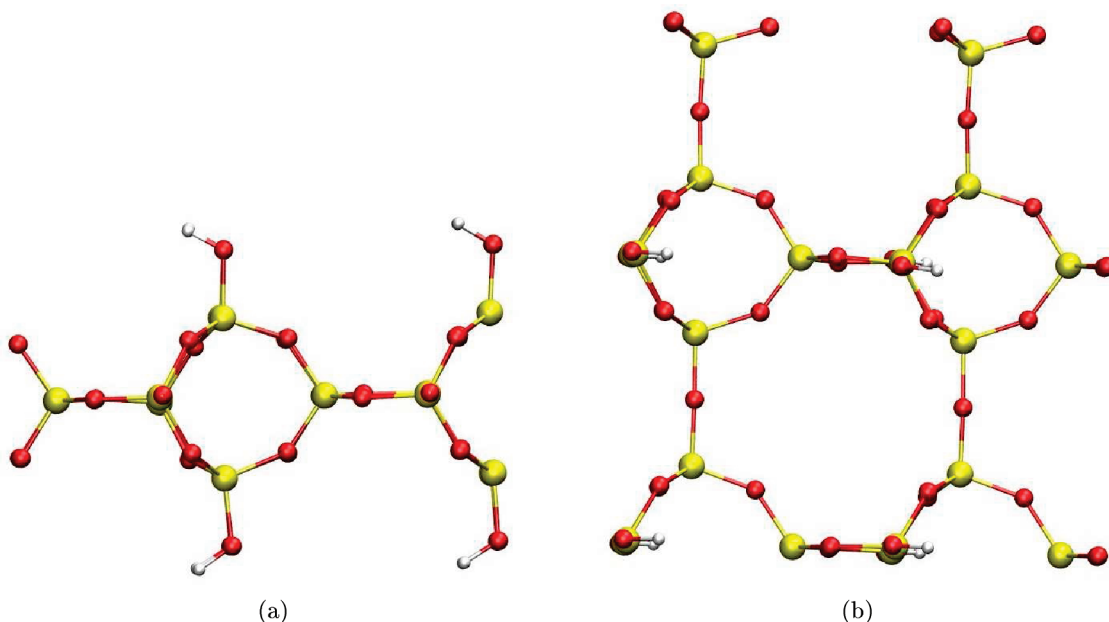
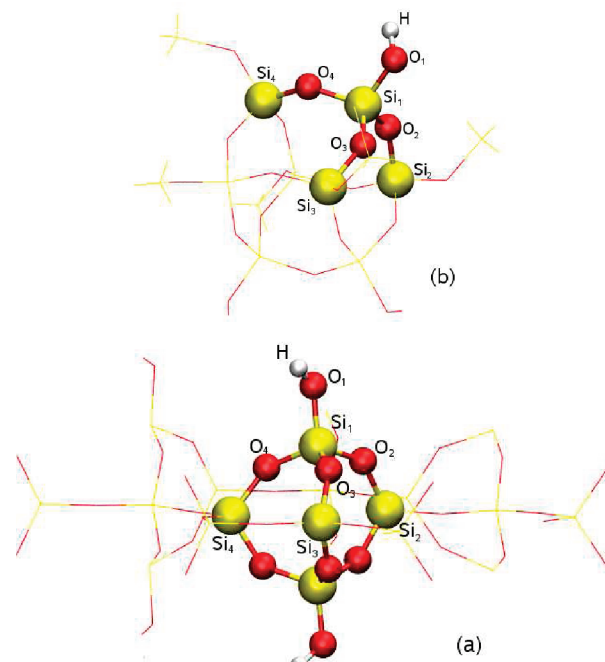


Figure 5. Edingtonite (100) (a) side view; (b) top view.

TABLE 3: Comparison of Different Structural Parameters between Edingtonite₁₀₀ (a) and c Model (b)

c model	edingtonite ₁₀₀
Distances (Å)	
H–O ₁	0.962
O ₁ –S ₁	1.645
S ₁ –O ₂	1.650
S ₁ –O ₃	1.657
S ₁ –O ₄	1.656
O ₂ –S ₂	1.656
O ₃ –S ₃	1.658
O ₄ –S ₄	1.653
Angles (°)	
H–O ₁ –S ₁	114.7
O ₁ –S ₁ –O ₂	106.0
O ₁ –S ₁ –O ₃	110.7
O ₁ –S ₁ –O ₄	109.6
S ₁ –O ₂ –S ₂	140.2
S ₁ –O ₃ –S ₃	139.0
S ₁ –O ₄ –S ₄	140.0
H–O ₁ –S ₁	118.9
O ₁ –S ₁ –O ₂	109.1
O ₁ –S ₁ –O ₃	107.5
O ₁ –S ₁ –O ₄	113.2
S ₁ –O ₂ –S ₂	139.4
S ₁ –O ₃ –S ₃	141.9
S ₁ –O ₄ –S ₄	139.2

Several attempts to coordinate $\text{La}(\text{NH}_2)_2$ on dehydrogenated silica surfaces have been considered. The grafting reaction on the **ac** cluster yielded two products, namely, $[\text{La}]@\text{ac-1}$ (Figure 6a) and $[\text{La}]@\text{ac-2}$ (Figure 6b). The reaction that leads to $[\text{La}]@\text{ac-1}$ is accompanied by the uptake of the hydrogen atom of the second silanol group by one amino group. The resulting lanthanum complex is bicoordinated to the surface, with lanthanum atom in a bridge position between two oxygen atoms, and it exhibits an ammonia molecule that makes an hydrogen bond with a siloxane oxygen. It is also possible to obtain a grafted complex without hydrogen transfer. The resulting compound, $[\text{La}]@\text{ac-2}$, lies 31.0 kcal. mol⁻¹ above $[\text{La}]@\text{ac-1}$. It should be noticed that structures with the lanthanum complex in a top position, that is, which is only coordinated to



the grafting SiO group without any additional interactions of siloxy or silanol oxygens, are not stable. All attempts for obtaining this type of coordination systematically led to a bridging form.

The differences observed in terms of geometry are confirmed by the NBO analysis. Indeed, this analysis shows the presence of two La–O bonds in the case of $[\text{La}]@\text{ac-1}$ and one La–O bond only in the case of $[\text{La}]@\text{ac-2}$. Differences are also obtained at the level of second-order perturbation analysis. For $[\text{La}]@\text{ac-2}$, it reveals a charge transfer from a $\sigma_{\text{Si}-\text{O}}$ bond to an empty d orbital of the metal center, which strengthens the La–O interaction. In addition, there is a weak donation from a lone pair of the two other oxygens, namely, the bridging oxygen ($\mu\text{-O}$) and O–H atoms, toward an empty d orbital of the metal

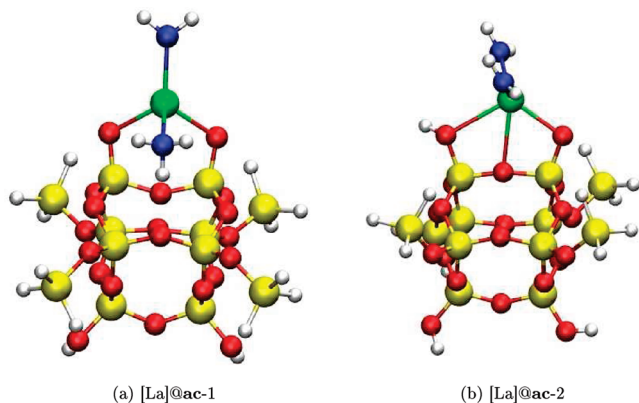


Figure 6. Possible structures obtained by grafting the lanthanum complex onto the ac model for silica.

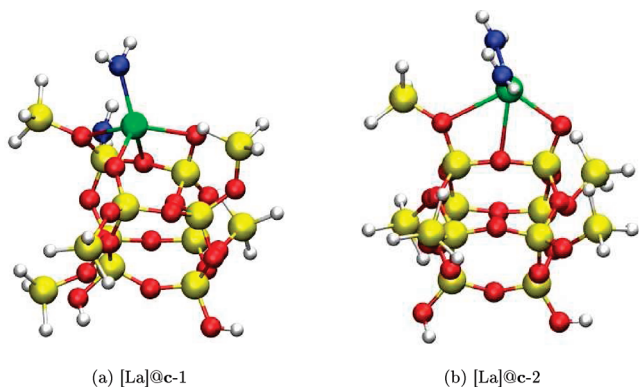


Figure 7. Possible structures obtained by grafting the lanthanum complex onto the c model for silica.

center. For [La]**@ac**-1, this analysis reveals only an additional charge transfer from the two $\sigma_{\text{Si}-\text{O}}$ bonds to empty d orbitals of the metal center.

Before looking at the reaction's products between the lanthanum catalyst and model **c**, we shall highlight that it is not possible to obtain hydrogenated ammonia ligands since no vicinal silanol group is present. The lanthanide complex is able to break the siloxane bridge, leading to structure $[\text{La}]@\text{c-1}$ (Figure 7a). Such breaking has previously been envisaged owing to experimental outcomes. We shall now focus on that structure. According to our model, one amino group is now directly bound to a silicon atom initially involved in the broken siloxane bond. The change of the N–La bonding type is also observed both by NBO analysis with no remaining $\text{La}\cdots\text{NH}_2$ bonding and in terms of metal–nitrogen distances, with R_2N –La bond lengths usually close to 2.2 Å, whereas the SiH_2N –La bond length is higher than 4 Å in $[\text{La}]@\text{c-1}$. The lanthanum complex can be considered bigrafted, with two short La–O distances (2.461 and 2.256 Å) but also in interaction with two other oxygens, with two longer La–O distances (2.692 and 2.732 Å). A second structure with a bridging monografted lanthanum, namely, $[\text{La}]@\text{c-2}$ (Figure 7b), has also been obtained. It is very similar to $[\text{La}]@\text{ac-2}$. $[\text{La}]@\text{c-1}$ is more stable than $[\text{La}]@\text{c-2}$ by 6.9 kcal·mol⁻¹ in relation with the Si–O bond breaking counter-balancing the formation of a strong La–O bond.

The NBO analysis of [La]@**c-2** confirms the similarity between this form and [La]@**ac-2** in terms of La–O bonding, with only one La–O bond. In the same way, the second-order perturbation analysis reveals an additional charge transfer from the $\sigma_{\text{Si}-\text{O}}$ bond to an empty d orbital of the metal center. In addition, there is a weak donation from a lone pair of the two

TABLE 4: Energy and Free Gibbs Energy of the Grafting Reaction of a Lanthanum Complex on ac and c Silica Surface Models

model	ΔE^0 (kcal·mol ⁻¹)	$\Delta_r G^0$ (kcal·mol ⁻¹)
[La] @ac-1	-70.1	-62.7
[La] @ac-2	-39.1	-34.7
[La] @c-1	-44.7	-35.3
[La] @c-2	-37.8	-32.4

other oxygens, namely the μ -O and O-H atoms, toward an empty d orbital of the metal center. Concerning [La]@ ϵ -1, the NBO analysis shows the existence of two La-O bonds, in agreement with a bicoordination of the lanthanum complex at the surface. The second-order perturbation analysis reveals a charge transfer of the two $\sigma_{\text{Si}-\text{O}}$ bond to an empty d orbital of the metal center as well as weak donation from a lone pair of the two other oxygens to an empty d orbital of the metal center.

Looking at the free Gibbs energies of these grafting reactions (Table 4), we can observe, that all reactions are exergonic, with $\Delta_f G^0$ ranging from -32 to -63 kcal \cdot mol $^{-1}$. These results qualitatively agree with the experimental data, which show an ability to easily graft lanthanide complexes onto SiO $_2$ -700 treated silica surfaces.

In general, in the case of the **c** model, the grafting reaction leads to a monografted lanthanide complex in a bridging position with two other weak La–O interactions, namely [La]**@c-2**. However, we have shown the existence of a thermodynamically more stable structure, [La]**@c-1**, which results from the breaking of a siloxane bridge by the transfer of a amino group to the silica surface. Despite our efforts, we were unable to find the transition state between the two structures on the potential energy surface. The barrier height is probably low, as a precaution to take into account the two structures for all reactivity calculations. In addition, note that the total energy of [La]**@ac** and [La]**@c** models cannot be directly compared owing to the different composition of the two systems. Both should be hereafter considered on the basis of their stability.

4.2. Which Cluster Model Is the More Realistic? Coor-

dination of a triphenylphosphine oxide ($O=PPh_3$) has been considered, on probe of the coordination of $Ln(NR_2)_3$ lanthanum complex. Rare-earth lanthanide complexes are known to react with triphenylphosphine oxide to afford monoadducts $[Ln(NR_2)_3(O=PPh_3)]$.⁷⁷ From an experimental point of view, the coordination of the $OPPh_3$ ligand is reversible: $OPPh_3$ sublimes away upon heating under vacuum. It indicates a certain degree of lability and therefore, to some extent, shows that $OPPh_3$ coordination strength can be affected by the coordination sphere of the grafted complex. The reaction of $OPPh_3$ with grafted rare-earth amides has been previously studied by R. M. Gauvin et al.¹¹ It leads to the formation of monoadducts of the type $[(\equiv Si-O)-Ln(NR_2)_2(O=PPh_3)]$, which have been characterized by IR and NMR. $OPPh_3$ has a clear vibrational ($C-H$, aromatic- C , and $O=P$) and spectroscopic (1H , ^{13}C , and ^{31}P) signature, this allows the comparison between theoretical and experimental data.

We have theoretically considered that coordination reaction in order to examine if the three models, namely, [La]⁺@ac-1, [La]⁺@c-1, and [La]⁺@c-2, remains qualitatively in agreement with the experimental spectroscopic data. In all cases the reaction is thermodynamically favorable, with Gibbs free energies equal to -18.0, -21.8, and -14.6 kcal·mol⁻¹ respectively.

The calculated vibrational C–H, aromatic–C, and O=P frequencies of the adsorbed OPPh₃ molecule are reported in Table 5. A good agreement between the theoretical and the

TABLE 5: Experimental and Calculated Values for the Vibrational Frequencies (in cm^{-1}) of OPPh_3 Molecule Coordinated at Different Grafted Lanthanum Complex

grafting mode	$\text{OPPh}_3@[\text{La}]@\text{ac-1}$	$\text{OPPh}_3@[\text{La}]@\text{c-1}$	$\text{OPPh}_3@[\text{La}]@\text{c-2}$	exp. ^a
$\nu_{\text{C}-\text{H}}$	[3071–3100]	[3068–3107]	[3068–3095]	~3066
$\nu_{\text{aromatic}-\text{C}}$	[1417–1592]	[1416–1591]	[1417–1592]	[1440–1593] ^b
$\nu_{\text{O}=\text{P}}$	1152	1121	1118	[1120–1180] ^b

^a Reference 11. ^b Expected but not detected band.

TABLE 6: Comparison between the Theoretical and the Experimental ^1H , ^{13}C , and ^{31}P NMR Chemical Shifts δ (in ppm) of OPPh_3 Molecule Coordinated at Different Grafted Lanthanum Complexes^a

grafting mode	$\text{OPPh}_3@[\text{La}]@\text{ac-1}$	$\text{OPPh}_3@[\text{La}]@\text{c-1}$	$\text{OPPh}_3@[\text{La}]@\text{c-2}$	exp. ^b	OPPh_3^c
$\delta_{\text{H}_{\text{phenyl}}}$	7.9	8.0	8.0	7.4	7.7
$\delta_{\text{C}_{\text{phenyl}}}$	124.8	124.6	124.7	128.4	124.7
	128.7	128.1	128.6	132.5	129.9
δ_{P}	47.6	41.9	46.3	39.1	25.7

^a ^1H and ^{13}C chemical shifts are given with respect to TMS (theoretical chemical shielding: 31.7 ppm/195.2 ppm respectively to ^1H and ^{13}C atoms). ^{31}P chemical shifts are given with respect to phosphoric acid (theoretical chemical shielding: 380.6 ppm).

^b Reference 11. ^c Free OPPh_3 ligand.

experimental stretching C–H (between 3068 and 3107 cm^{-1} vs ~3066 cm^{-1}) and aromatic–C bands (between 1417 and 1592 cm^{-1} vs [1440–1593] cm^{-1}) is obtained whatever the model.⁷⁸ The vibrational stretching mode of the O=P bond, experimentally expected (but not observed) between 1120 and 1180 cm^{-1} , is obtained in this domain with the three grafting modes.

As a consequence, it is not possible to determine by studying only this vibrational property if a specific grafting mode is more realistic. Another way to discriminate between models is to compare the theoretical and experimental ^1H , ^{13}C , and ^{31}P NMR chemical shifts of the coordinated OPPh_3 molecule, as reported in Table 6. Concerning the phenyl groups, the hydrogen atoms give rise to a single resonance observed at 7.41 ppm. Our calculation yields chemical shift values in a narrow domain and close to experiments: 7.9, 8.0, and 8.0 ppm, respectively, for $\text{OPPh}_3@[\text{La}]@\text{ac-1}$, $\text{OPPh}_3@[\text{La}]@\text{c-1}$, and $\text{OPPh}_3@[\text{La}]@\text{c-2}$. The ^{13}C CP-MAS spectrum displays two peaks for the aromatic carbons, $\delta = 128.4$ and 132.5 ppm. The calculated chemical shifts are obtained between 124.6 and 124.8 ppm and between 128.1 and 128.7 ppm, respectively, in very good agreement with experiments. Not only are the theoretical and experimental values close, but the two values are separated by 4 ppm in both cases. Finally, the ^{31}P MAS NMR spectrum displays one singlet at 39.1 ppm. As can be seen in Table 6, the calculated chemical shift for the phosphorus atom of the OPPh_3 molecule for the different considered structures is between 41.9 and 47.6 ppm. It could be tempting, on the basis of the ^{31}P NMR data, to consider $[\text{La}]@\text{c-1}$ as the most relevant model. However, the maximum difference between theoretical and experimental values (22%) calculated for $\text{OPPh}_3@[\text{La}]@\text{ac-1}$ is not so far to the reasonable accuracy domain considered for this type of calculations, that is, ~10–20%. Note that the difference observed in the chemical shift value of phosphorus for the three structures is consistent with the structural differences associated to the coordination of OPPh_3 . To assess these differences we have considered three structural parameters: the La–O_{OPPh₃} distance, the La–O_{OPPh₃}–P angle, and finally the ligand cone angle or Tolman's angle,⁷⁹ which provides information about the pyramidalization of the phosphorus atom and the steric hindrance of the three ligands. The values for these three

TABLE 7: Different Structural Parameters of the Coordination of OPPh_3 Molecule on $[\text{La}]@\text{ac-1}$, $[\text{La}]@\text{c-1}$, and $[\text{La}]@\text{c-2}$ ^a

grafting mode	$\text{OPPh}_3@[\text{La}]@\text{ac-1}$	$\text{OPPh}_3@[\text{La}]@\text{c-1}$	$\text{OPPh}_3@[\text{La}]@\text{c-2}$
La–O _{OPPh₃}	2.484	2.414	2.463
La–O _{OPPh₃} –P	145.1	159.8	151.9
ligand cone	170.8	181.9	176.9

^a La–O_{OPPh₃} distance given in Å. La–O_{OPPh₃}–P and ligand cone angles given in degrees.

parameters for the different models are reported in Table 7. In the case of $[\text{La}]@\text{c-1}$, the transfer of the amino group on the surface model allow a decrease of the steric hindrance around the metal and the coordination site will be easily accessible. From a structural point of view, this accessibility leads to a ligand cone angle close to that of the free OPPh_3 molecule: 181.9 vs 180.1, respectively. For $[\text{La}]@\text{ac-1}$ and $[\text{La}]@\text{c-2}$, the ligand cone angle is slightly smaller, which indicates a greater pyramidalization around the phosphorus atoms in order to increase the accessibility to the metal center. For the same reasons, the La–O_{OPPh₃} distance is shorter in the case of $[\text{La}]@\text{c-1}$ than for $[\text{La}]@\text{ac-1}$ and $[\text{La}]@\text{c-2}$ (2.414 Å, 2.484, and 2.463 Å, respectively). These differences in the local environment of the phosphorus atom may explain the differences between the calculated chemical shifts of $\text{OPPh}_3@[\text{La}]@\text{ac-1}$, $\text{OPPh}_3@[\text{La}]@\text{c-1}$, and $\text{OPPh}_3@[\text{La}]@\text{c-2}$.

Finally, we have also considered the influence of the phenyl rotation on the ^{31}P chemical shift. It is an almost barrierless rotation, with $\Delta G_{\text{rot}}^{\ddagger} = 4 \text{ kcal mol}^{-1}$. The influence on the chemical shift of the phosphorus atom is very moderate, although it gets closer to experiments, with a shielded atom of approximately 2 ppm.

4.3. Grafted Lanthanum Complex on the Edingtonite Model. We have also studied the grafting reaction of a lanthanum complex on the edingtonite₁₀₀ periodic model. The grafting reaction is the same as previously considered:



Several attempts to coordinate $\text{La}(\text{NH}_2)_2$ on the edingtonite₁₀₀ model have been envisaged. The grafting reaction on this model yielded different products, but only the most stable forms, namely, $[\text{La}]@\text{ed}_{100-1}$ (Figure 8a) and $[\text{La}]@\text{ed}_{100-2}$ (Figure 8b) are shown here. The grafting reaction is thermodynamically favorable in both cases, with $\Delta E = -42.8$ and $-31.5 \text{ kcal mol}^{-1}$, respectively, for $[\text{La}]@\text{ed}_{100-1}$ and $[\text{La}]@\text{ed}_{100-2}$.

As we observe with $[\text{La}]@\text{c-1}$, the lanthanum complex is able to break the siloxane bridge. With an edingtonite₁₀₀ model, the grafting reaction involving the breaking of a siloxane bridge is also possible and leads to the structure $[\text{La}]@\text{ed}_{100-2}$ (Figure 8b). The lanthanum complex can be considered as bigrafted, with two short La–O distances (2.287 and 2.196 Å), but also in interaction with another oxygen atom, with a longer La–O distance (2.788 Å). A second structure with a bridging monograft-

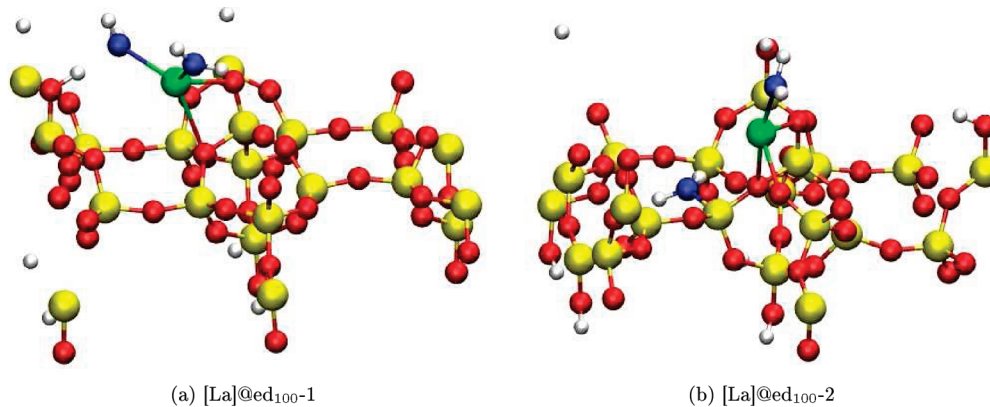


Figure 8. Possible structures obtained by grafting the lanthanum complex onto the edingtonite₁₀₀ model for silica.

ed lanthanum, namely, [La]@ed₁₀₀-1 (Figure 8a), has also been obtained. It is similar to [La]@c-2, which has a significantly shorter La—O bond length (2.278 Å) but also is in interaction with another oxygen atom, with a longer La—O distance (2.769 Å). It will be hereafter considered as monografted. However, contrarily to the molecular models, this bridging structure is more stable than [La]@ed₁₀₀-2 by 11.2 kcal·mol⁻¹. This stability difference between the molecular and periodic structures concerning the mono- and bigrafted complexes can be explained from a structural point of view. Indeed, the origin of this difference is functional-independent,⁸⁰ but several differences are observed in the grafting reaction on the edingtonite₁₀₀ model and the c model. As we saw earlier, during the grafting reaction of the lanthanum complex on the edingtonite₁₀₀ and the c models, it is not possible to uptake the hydrogen atom of a vicinal silanol group by one amino group, as observed with ac. However, with the edingtonite₁₀₀ model, the presence of a neighbor second silanol group allows the creation of a hydrogen bond between that silanol group and one amino ligand of the lanthanum complex. As can be seen on Figure 8a, this interaction leads to a pyramidalization of the nitrogen atom of the amino group and stabilizes this type of grafting. Although the two silanol groups are separated by 6 Å, such long distance interaction can occur and could be accounted for in the context of molecular calculations with a larger cluster model. Concerning the [La]@ed₁₀₀-2 structure, we can also note some differences compared to [La]@c-2. Although the complex is bigrafted in [La]@ed₁₀₀-2, it also interacts with a third oxygen atom, whereas for [La]@c-2 two interactions only were observed. The lowering La—O interaction, in [La]@ed₁₀₀-2, together with the creation of an hydrogen bond, in [La]@ed₁₀₀-1, could explain the difference observed in the relative stability between [La]@ed₁₀₀-1 and [La]@ed₁₀₀-2 on one hand and [La]@c-1 and [La]@c-2 on the other hand.

It should also be noted that with both molecular and periodic models, grafting in a top position is not favorable. Indeed, in the case of molecular systems we have not found a minimum corresponding to this form, whereas for the periodic structure with a lanthanum complex grafted in, a top position is 14.0 kcal·mol⁻¹ less stable than [La]@ed₁₀₀-1.

5. Conclusion

In conclusion, we have tried to create realistic molecular models for a SiO₂–700 surface. After a first selection based on the rigidity of the ligand, the surface density of silanol groups, and IR frequencies of the hydroxyl groups of the silanols, two possible models of the surface have henceforth been considered. The thermodynamics of a grafting reaction of lanthanum

catalysts on these models has also been investigated. This reaction leads to thermodynamically stable structures that reveal different types of grafting: monografted ([La]@c-2), bigrafted ([La]@ac-1), or bigrafted after breaking of an Si—O—Si bridge ([La]@c-1). The molecular model c, with an isolated silanol group, is also compared to a periodic silica surface model. Despite a slight disagreement between the molecular and periodic models, it should be underlined that they provide similar conclusions: grafting in a top position is not favorable, and there are two relevant grafting modes when the coordination site is an isolated silanol: on one hand a monografted complex in a bridging position ([La]@c-2 and [La]@ed₁₀₀-1), and on the other hand a bigrafted catalyst by the break of a siloxane bridge ([La]@c-1 and [La]@ed₁₀₀-2). Similarly to experimental approaches, coordination of triphenylphosphine oxide (O=PPPh₃) has also been considered as a probe of the grafting mode. A good agreement between the theoretical and the experimental spectroscopic values have systematically been found, but none of the models seem to be more relevant. In summary, it is possible that all forms of grafted silica surface coexist, so that it could be necessary to consider the different models ac and c (see Figure 3) in future reactivity studies that would involve such complexes.

Acknowledgment. The french ANR is gratefully acknowledged for financial support (SIDERUS project, ANR-08-BLAN-0010-02). We also thank the CALcul en MIDI-Pyrénées (CALMIP-p0833 project) for generous allocations of computer time. This work was performed using HPC resources from GENCI-[CINES] (Grant 2010-7211). L. M. is a member of the Institut Universitaire de France (IUF). We thank Dr. Noemi Barros for carefully reading the manuscript. Dr. Christophe Copéret is gratefully acknowledged for stimulating discussions.

Supporting Information Available: Energies and Cartesian coordinates for all molecular systems and POSCAR files of periodic systems. This material is available free of charge via the Internet at <http://pubs.acs.org>.

References and Notes

- Zwijnenburg, M. A.; van Alsenoy, C.; Maschmeyer, T. *J. Phys. Chem. A* **2002**, *106*, 12376–12385.
- Antonietti, J.-M.; Michalski, M.; Heiz, U.; Jones, H.; Lim, K. H.; Rösch, N.; Vitto, A. D.; Pacchioni, G *Phys. Rev. Lett.* **2005**, *94*, 213402.
- Rhers, B.; Salameh, A.; Baudoin, A.; Quadrelli, E. A.; Taoufik, M.; Copéret, C.; Lefebvre, F.; Basset, J.-M.; Solans-Monfort, X.; Eisenstein, O.; Lukens, W. W.; Lopez, L. P. H.; Sinha, A.; Schrock, R. R. *Organometallics* **2006**, *25*, 3554–3557.
- Blanc, F.; Basset, J.-M.; Copéret, C.; Sinha, A.; Tonzetich, Z. J.; Schrock, R. R.; Solans-Monfort, X.; Clot, E.; Eisenstein, O.; Lesage, A.; Emsley, L. *J. Am. Chem. Soc.* **2008**, *130*, 5886–5900.

- (5) Civalleri, B.; Garrone, E.; Ugliengo, P. *Chem. Phys. Lett.* **1999**, *299*, 443–450.
- (6) Casanovas, J.; Illas, F.; Pacchioni, G. *Chem. Phys. Lett.* **2000**, *326*, 523–529.
- (7) VigneMaeder, F.; Sautet, P. *J. Phys. Chem. B* **1997**, *101*, 8197–8203.
- (8) Ginhoven, R. V.; Hjalmarson, H.; Edwards, A.; Tuttle, B. *Nucler. Inst. Met. Phys. Res. B* **2006**, *250*, 274–278.
- (9) Lim, K. H.; Zakharia, O.; Shor, A. M.; Rösch, N. *Chem. Phys. Lett.* **2007**, *448*, 280–286.
- (10) Chuang, I.-S.; Maciel, G. E. *J. Phys. Chem. B* **1997**, *101*, 3052–3064.
- (11) Gauvin, R. M.; Delevoye, L.; Hassan, R. A.; Keldenich, J.; Mortreux, A. *Inorg. Chem.* **2007**, *46*, 1062–1070.
- (12) Gauvin, R. M.; Mortreux, A. *Chem. Commun.* **2005**, *9*, 1146–1148.
- (13) Gauvin, R. M.; Chenal, T.; Hassan, R. A.; Abbad, A.; Mortreux, A. *J. Mol. Cat. A: Chemical* **2006**, *257*, 31–40.
- (14) Solans-Monfort, X.; Filhol, J.-S.; Copéret, C.; Eisenstein, O. *New. J. Chem.* **2006**, *30*, 842–850.
- (15) Bradley, D. C.; Ghotra, J. S.; Hart, F. A. *J. Chem. Soc., Dalton Trans.* **1973**, 1021–1023.
- (16) Q.Shen,; Huang, W.; Wang, J.; Zhou, X. *Organometallics* **2008**, *27*, 301–303.
- (17) Frisch, M. J.; Trucks, G. W.; Schlegel, H. B.; Scuseria, G. E.; Robb, M. A.; Cheeseman, J. R.; Montgomery, J. A., Jr.; Vreven, T.; Kudin, K. N.; Burant, J. C.; Millam, J. M.; Iyengar, S. S.; Tomasi, J.; Barone, V.; Mennucci, B.; Cossi, M.; Scalmani, G.; Rega, N.; Petersson, G. A.; Nakatsuji, H.; Hada, M.; Ehara, M.; Toyota, K.; Fukuda, R.; Hasegawa, J.; Ishida, M.; Nakajima, T.; Honda, Y.; Kitao, O.; Nakai, H.; Klene, M.; Li, X.; Knox, J. E.; Hratchian, H. P.; Cross, J. B.; Bakken, V.; Adamo, C.; Jaramillo, J.; Gomperts, R.; Stratmann, R. E.; Yazayev, O.; Austin, A. J.; Cammi, R.; Pomelli, C.; Ochterski, J. W.; Ayala, P. Y.; Morokuma, K.; Voth, G. A.; Salvador, P.; Dannenberg, J. J.; Zakrzewski, V. G.; Dapprich, S.; Daniels, A. D.; Strain, M. C.; Farkas, O.; Malick, D. K.; Rabuck, A. D.; Raghavachari, K.; Foresman, J. B.; Ortiz, J. V.; Cui, Q.; Baboul, A. G.; Clifford, S.; Cioslowski, J.; Stefanov, B. B.; Liu, G.; Liashenko, A.; Piskorz, P.; Komaromi, I.; Martin, R. L.; Fox, D. J.; Keith, T.; Al-Laham, M. A.; Peng, C. Y.; Nanayakkara, A.; Challacombe, M.; Gill, P. M. W.; Johnson, B.; Chen, W.; Wong, M. W.; Gonzalez, C.; Pople, J. A. *Gaussian 03, revision B.05*; Gaussian, Inc.: Wallingford, CT, 2003.
- (18) Perdew, J. P. In *Electronic Structure of Solids*; Ziesche, P., Eschrig, H., Eds.; Akademie: Berlin, 1991; Ch Unified Theory of Exchange and Correlation Beyond the Local Density Approximation.
- (19) Perdew, J. P.; Burke, K.; Wang, Y. *Phys. Rev. B* **1996**, *54*, 16533–16539.
- (20) Burke, K.; Perdew, J. P.; Wang, Y. In *Electronic Density Functional Theory: Recent Progress and New Directions*; Dobson, J. F., Vignale, G., Das, M. P., Eds.; Plenum: New-York, 1998; Ch Derivation of a Generalized Gradient Approximation: The PW91 Density Functional.
- (21) Perdew, J. P.; Chevary, J. A.; Vosko, S. H.; Jackson, K. A.; Pederson, M. R.; Singh, D. J.; Fiolhais, C. *Phys. Rev. B* **1992**, *46*, 6671–6687.
- (22) Perdew, J. P.; Burke, K.; Wang, Y. *Phys. Rev. B* **1998**, *57*, 14999.
- (23) Perdew, J. P.; Chevary, J. A.; Vosko, S. H.; Jackson, K. A.; Pederson, M. R.; Singh, D. J.; Fiolhais, C. *Phys. Rev. B* **1993**, *48*, 4978.
- (24) Küechle, W.; Dolg, M.; Stoll, H.; Preuss, H. *Mol. Phys.* **1991**, *74*, 1245–1263.
- (25) Harihara, P. C.; Pople, J. A. *Theor. Chim. Acta* **1973**, *28*, 213–222.
- (26) Hehre, W. J.; Ditchfield, R.; Pople, J. A. *J. Chem. Phys.* **1972**, *56*, 2257–2261.
- (27) London, F. *J. Phys. Radium* **1937**, *8*, 397–409.
- (28) McWeeny, R. *Phys. Rev.* **1962**, *126*, 1028–1034.
- (29) Ditchfield, R. *Mol. Phys.* **1974**, *27*, 789–807.
- (30) Dodds, J. L.; McWeeny, R.; Sadlej, A. *J. Mol. Phys.* **1977**, *34*, 1779–1791.
- (31) Woliński, K.; Hinton, J. F.; Pulay, P. *J. Am. Chem. Soc.* **1990**, *112*, 8251–8260.
- (32) Reed, A. E.; Weinhold, F. *J. Chem. Phys.* **1983**, *78*, 4066–4074.
- (33) Reed, A. E.; Curtiss, L. A.; Weinhold, F. *Chem. Rev.* **1988**, *88*, 899–926.
- (34) Kresse, G.; Furthmüller, J. *Comput. Mater. Sci.* **1996**, *6*, 15–50.
- (35) Kresse, G.; Furthmüller, J. *Phys. Rev. B* **1996**, *54*, 11169–11186.
- (36) Blöchl, P. E. *Phys. Rev. B* **1994**, *50*, 17953–17979.
- (37) Kresse, G.; Joubert, D. *Phys. Rev. B* **1999**, *59*, 1758–1775.
- (38) Perdew, J. P.; Burke, K.; Emzerhof, M. *Phys. Rev. Lett.* **1996**, *77*, 3865.
- (39) Monkhorst, H. J.; Pack, J. D. *Phys. Rev. B* **1976**, *13*, 5188–5192.
- (40) Blöchl, P. E.; Jepsen, O.; Andersen, O. K. *Phys. Rev. B* **1994**, *49*, 16223–16233.
- (41) Swamy, V.; Saxena, S. K.; Sundman, B.; Zhang, J. *J. Geophys. Res.* **1994**, *99*, 11787–11794.
- (42) Mao, H.; Sundman, B.; Wand, Z.; Saxena, S. K. *J. Alloys Comp.* **2001**, *327*, 253–262.
- (43) Thiel, P. A.; Madey, T. E. *Surf. Sci. Rep.* **1987**, *7*, 211–385.
- (44) Henderson, M. A. *Surf. Sci. Rep.* **2002**, *46*, 1–308.
- (45) Leed, E. A.; Sofo, J. O.; Pantano, C. G. *Phys. Rev. B* **2005**, *72*, 155427.
- (46) Ma, Y.; Foster, A. S.; Nieminen, R. M. *J. Chem. Phys.* **2005**, *122*, 144709.
- (47) Yang, J.; Wang, E. G. *Curr. Opin. Solid State Mater. Sci.* **2006**, *10*, 33–39.
- (48) Blitz, J. P.; Murphy, R. S. S.; Leyden, D. E. *J. Am. Chem. Soc.* **1987**, *109*, 7141–7145.
- (49) der Voort, P. V.; Vansant, E. F. *Pol. J. Chem.* **1997**, *71*, 550–567.
- (50) Zhao, X. S.; Lu, G. Q. *J. Phys. Chem. B* **1998**, *102*, 1556–1561.
- (51) Humbert, B. *J. Non-Cryst. Solids* **1995**, *191*, 29–37.
- (52) Gnado, J.; Dhamelincourt, P.; Pélegreis, C.; Traisnel, M.; Mayot, A. L. M. *J. Non-Cryst. Solids* **1996**, *208*, 247–258.
- (53) Czuryszkiewicz, T.; Ahvenlammi, J.; Kortesuo, P.; Ahola, M.; Kleitz, F.; Jokinen, M.; Linden, M.; Rosenholm, J. B. *J. Non-Cryst. Solids* **2002**, *306*, 1–10.
- (54) Legrand, A. P.; Hommel, H.; Tuel, A.; Vidal, A.; Balard, H.; Papirer, E.; Levitz, P.; Czernichowski, M.; Erre, R.; Damme, H. V. *Adv. Colloid Interface Sci.* **1990**, *33*, 91–330.
- (55) Mueller, R.; Kammler, H. K.; Wegner, K.; Pratsinis, S. E. *Langmuir* **2003**, *19*, 160–165.
- (56) Fischer, K. *Angew. Chem., Int. Ed. Eng.* **1935**, *26*, 394–396.
- (57) Gilman, H.; Miller, L. S. *J. Am. Chem. Soc.* **1951**, *73*, 2367–2368.
- (58) Brown, F. F. *J. Am. Chem. Soc.* **1965**, *87*, 4317–4324.
- (59) Armistead, C. G.; Tyler, A. J.; Hambleton, F. H.; Mitchell, S. A.; Hockey, J. A. *J. Phys. Chem.* **1969**, *73*, 3947–3953.
- (60) Derouet, D.; Forgeard, S.; Brosse, J.-C.; Emery, J.; Buzare, J.-Y. *J. Polym. Sci., Part A* **1998**, *36*, 437–453.
- (61) Zhuravlev, L. T. *Colloid Surface A* **2000**, *173*, 1–38.
- (62) Sindorf, D. W.; Maciel, G. E. *J. Am. Chem. Soc.* **1983**, *105*, 1487–1493.
- (63) Zhuravlev, L. T. *Langmuir* **1987**, *3*, 316.
- (64) Tsubokawa, N.; Saitoh, K.; Shirai, Y. *Polym. Bull.* **1995**, *35*, 399–406.
- (65) Tuel, A.; Hommel, H.; Legrand, A. P.; Chevallier, Y.; Morawski, J. C. *Colloids Surf.* **1990**, *45*, 413–426.
- (66) Vansant, E. F.; der Voort, P. V.; Vrancken, K. C. *Characterization and Chemical Modification of the Silica Surface*; Elsevier: Amsterdam, 1996.
- (67) Feher, F. J.; Newman, D. A.; Walzer, J. F. *J. Am. Chem. Soc.* **1989**, *111*, 1741–1748.
- (68) Wolfgang, A.; Herrmann, W. A.; Anwander, R.; Dufaud, V.; Scherer, W. *Angew. Chem., Int. ed. Eng.* **1994**, *33*, 1285–1286.
- (69) Feher, F. J.; Budzichowski, T. A. *Polyhedron* **1995**, *14*, 3239–3253.
- (70) Duchateau, R. *Chem. Rev.* **2002**, *102*, 3525–3542.
- (71) Chuang, I.-S.; Maciel, G. J. *J. Am. Chem. Soc.* **1996**, *118*, 401–406.
- (72) Baraille, I.; Loudet, M.; Laccombe, S.; Cardy, H.; Pisani, C. *J. Mol. Struct. Theochem* **2003**, *620*, 291–300.
- (73) Civalleri, B.; Casassa, S.; Garrone, E.; Pisani, C.; Ugliengo, P. *J. Phys. Chem. B* **1999**, *103*, 2165–2171.
- (74) Tosoni, S.; Pascale, F.; Ugliengo, P.; Orlando, R.; Saunders, V. R.; Dovesi, R. *Mol. Phys.* **2005**, *103*, 2549–2558.
- (75) Anwander, R.; Roesky, R. *J. Chem. Soc., Dalton Trans.* **1997**, *2*, 137–138.
- (76) Anwander, R.; Runte, O.; Eppinger, J.; Gestberger, G.; Herdtweck, H.; Spiegler, M. *J. Chem. Soc., Dalton Trans.* **1998**, *5*, 847–858.
- (77) Bradley, D. C.; Ghotra, J. S.; Hart, F. A.; Hursthouse, M. B.; Raithby, P. R. *J. Chem. Soc., Dalton Trans.* **1977**, 1166–1172.
- (78) Aromatic rings are expected to freely rotate around the C–P axis, which should yield to an averaging of the calculated C–H stretching frequencies.
- (79) Tolman, C. A. *Chem. Rev.* **1977**, *77*, 313–348.
- (80) Full geometry optimization on [La]@c-1 and [La]@c-2 performed at the PBE (the functional used within periodic calculations) and B3PW91 (the one considered with the cluster models) levels of calculation agree for their relative energy ordering (9.4 vs 6.9 kcal·mol⁻¹).